Simulation and Implementation of Thyristor controlled reactor and Shunt Hybrid Power Filter

[1]Swapnil S. Motaphale, [2]Dr. N.M.Lokhande

[1]ME Electrical (Power System), [2]Professor

***Abstract*: This paper proposes the implementation of the comparative analysis of the with conventional power system arrangement to the steady state and dynamic state of the combined system of a Thyristor-controlled reactor (TCR) and a shunt hybrid power filter (SHPF), for the process of limiting the total harmonic reduction and concept of reactive power compensation. The SHPF is the combination of a small-rating active power filter (APF) and a fifth-harmonic-tuned LC passive filter. The tuned passive filter and the TCR form a shunt passive filter (SPF) to compensate reactive power. The small-rating APF is used to improve the filtering characteristics of SPF and to suppress the possibility of resonance between the SPF and line inductances. A proportional–integral controller was used, and a triggering alpha was extracted using a lookup table to control the tcr. Total circuit configuration is simulated and implemented using MATLAB 2016a and it is analyzed in power graphical user interfacing environment and the total harmonic distortion is calculated by the use of the fast fourier transformation technique in powergui.**

1. Introduction

Rising energy cost and a greater sensitivity to environmental impact of new transmission lines necessitated the search and application of new controllers to minimize losses and maximize the stable power transmission capacity of existing lines. Nonlinear loads cause significant harmonic currents with poor input power factor (PF), which create serious problems at the power supply system. Traditionally, passive filters have been used to eliminate current harmonics of the supply network. However, these devices suffer from resonance. Recently, thyristor-switched filters (TSFs), which contain several groups of passive filters, have been used to compensate reactive power . The compensation amount of TSFs can be adjusted with the variation of load power . However, the parallel and the series resonance could occur between TSF and grid impedance. Active filters were developed to mitigate problems of passive filters [3]–[5]. They are more effective in harmonic compensation and have good performance [6]–[8]. However, the costs of active filters are relatively high for large scale system and require high power converter ratings [9], [10]. Hybrid filters effectively soften the problems of the passive filter and an active filter solution and provide cost-effective harmonic compensation, particularly for high-power nonlinear loads.

Many control techniques such as instantaneous reactive power theory, synchronous rotating reference frame, sliding-mode controllers, neural network techniques, nonlinear control, feedforward control, Lyapunov function- based control, etc., have been used to improve the performance of the active and hybrid filters. Several filter topologies for compensating harmonics and reactive power have been reported in the literature In, a multiconverter conditioner topology formed by an active conditioner operating in parallel with a hybrid conditioner has been proposed. The hybrid conditioner consists of one or more passive filters in series with a low-rated active power filter (APF). The conditioner compensates harmonic distortion, imbalance, and reactive power in three-phase four-wire systems. This topology constitutes an effective solution at high-power levels, which is cost-effective because of the kilovoltampere rating reduction of the inverters. A hybrid configuration based on the combination of a three-phase three-level neutral point clamped (NPC) inverter and a series connection of a three-level H-bridge inverter with a novel control scheme to control the floating voltage source of the H-bridge stage has been presented . In this topology, the NPC inverter is used to supply the total active power while the H-bridges operate as series active filters for the harmonic compensation of the NPC output voltage.

The rating of the series active filter is reduced because the latter provides only the reactive power for the operation of the floating capacitor. In , a combination of a thyristor controlled reactor (TCR) and a resonant impedance-type hybrid APF for harmonic cancellation, load balancing, and reactive power compensation has been proposed. The control strategy of the system is based on the voltage vector transformation for compensating the negative-sequence current caused by the unbalance load without using phase-locked loops. A predictive current controller based on the Smith predictor is proposed to compensate the generalized current delay. A combined system of a static var compensator (SVC) and a small-rated APF for harmonic suppression and reactive power compensation has been reported . The SVC consists of a Y-connected passive power filter and a delta-connected TCR. The APF is used to eliminate harmonic currents and to avoid resonance between the passive power filters and the grid impedance. In this paper, a new combination of a shunt hybrid power filter (SHPF) and a TCR (SHPF-TCR compensator) is proposed to suppress current harmonics and compensate the reactive power generated from the load. The hybrid filter consists of a series connection of a small-rated active filter and a fifth-tuned LC passive filter. In the proposed topology, the major part of the compensation is supported by the passive filter and the TCR while the APF is meant to improve the filtering characteristics and damps the resonance, which can occur between the passive filter, the TCR, and the source impedance.

The shunt APF when used alone suffers from the high kilovoltampere rating of the inverter, which requires a lot of energy stored at high dc-link voltage. On the other hand, as published by some authors , the standard hybrid power filter is unable to compensate the reactive power because of the behavior of the passive filter. Hence, the proposed combination of SHPF and TCR compensates for unwanted reactive power and harmonic currents. In addition, it reduces significantly the volt-ampere rating of the APF part. The control method of the combined compensator is presented. A control technique is proposed to improve the dynamic response and decrease the steady-state error of the TCR. It consists of a PI controller and a lookup table to extract the required firing angle to compensate a reactive power consumed by the load. A nonlinear control of SHPF is developed for current tracking and voltage regulation purposes.

It is based on a decoupled control strategy, which considers that the controlled system may be divided into an inner fast loop and an outer slow one. The currents injected by the SHPF are controlled in the synchronous orthogonal dq frame using a decoupled feedback linearization control method. The dc bus voltage is regulated using an output feedback linearization control. The SHPF can maintain the low level of dc bus voltage at a stable value below 50 V. The proposed nonlinear control scheme has been simulated and validated experimentally to compute the performance of the proposed SHPF-TCR compensator with harmonic and reactive power compensation and analysis through the total harmonic distortion (THD) of the source and the load current. The proposed methodology is tested for a wide range of loads as discussed further. Simulation and experimental results show that the proposed topology is suitable for harmonic suppression and reactive compensation.

.

2. SYSTEM CONFIGURATION OF SHPF-TCR COMPENSATOR

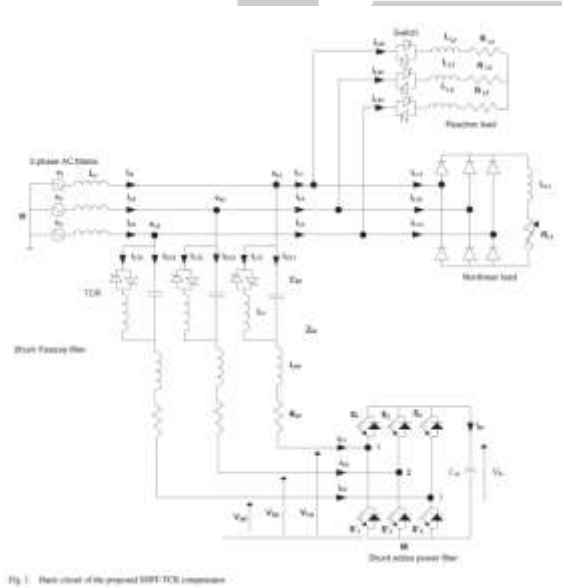

Fig. 1 shows the topology of the proposed combined SHPF and TCR. The SHPF consists of a small-rating APF connected in series with a fifth-tuned LC passive filter. The APF consists of a three-phase full-bridge voltage-source pusle width modulation (PWM) inverter with an input boost inductor (Lpf,Rpf) and a dc bus capacitor (Cdc). The APF sustains very low fundamental voltages and currents of the power grid, and thus, its rated capacity is greatly reduced. Because of these merits, the presented combined topology is very appropriate in compensating reactive power and eliminating harmonic currents in power system. The tuned passive filter in parallel with TCR forms a shunt passive filter (SPF). This latter is mainly for fifth harmonic compensation and PF correction. The small-rating APF is used to filter harmonics generated by the load and the TCR by enhancing the compensation characteristics of the SPF aside from eliminating the risk of resonance between the grid and the SPF. The TCR goal is to obtain a regulation of reactive power. The set of the load is a combination of a three phase diode rectifier and a three-phase star-connected resistive inductive linear load.

3. MODELING AND CONTROL STRATEGY

3.1 Modeling of SHPF

The system equations are first elaborated in 123 reference frame. Using Kirchhoff's voltage law, one can write

$$\begin{aligned}
v_{s1} &= L_{PF}\frac{di_{c1}}{dt} + R_{PF}i_{c1} + v_{CPF1} + v_{1M} + v_{MN}\\
v_{s2} &= L_{PF}\frac{di_{c2}}{dt} + R_{PF}i_{c2} + v_{CPF2} + v_{2M} + v_{MN}\\
v_{s3} &= L_{PF}\frac{di_{c3}}{dt} + R_{PF}i_{c3} + v_{CPF3} + v_{3M} + v_{MN}\\
v_{CPF1} &= L_T\frac{di_{c1}}{dt} - C_{PF}L_T\frac{d^2v_{CPF1}}{dt^2}\\
v_{CPF2} &= L_T\frac{di_{c2}}{dt} - C_{PF}L_T\frac{d^2v_{CPF2}}{dt^2}\\
v_{CPF3} &= L_T\frac{di_{c3}}{dt} - C_{PF}L_T\frac{d^2v_{CPF3}}{dt^2}\\
\frac{dv_{dc}}{dt} &= \frac{1}{C_{dc}}i_{dc}.
\end{aligned} \tag{1}$$

The switching function ck of the kth leg of the converter (for k = 1, 2, 3) is defined as

$$c_k = \begin{cases} 1, & \text{if } S_k \text{ is On and } S_k' \text{ is Off} \\ 0, & \text{if } S_k \text{ is Off and } S_k' \text{ is On.} \end{cases} \tag{2}$$

A switching state function dnk is defined as

$$d_{nk} = \left(c_k - \frac{1}{3}\sum_{m=1}^{3} c_m\right)_n. \tag{3}$$

Moreover, the absence of the zero sequence in the ac currents and voltages and in the [dnk] functions leads to the following transformed model in the three-phase coordinates [15]:

$$L_{PF}\frac{di_{c1}}{dt} = -R_{PF}i_{c1} - d_{n1}v_{dc} - v_{CPF1} + v_{s1}$$
$$L_{PF}\frac{di_{c2}}{dt} = -R_{PF}i_{c2} - d_{n2}v_{dc} - v_{CPF2} + v_{s2}$$
$$L_{PF}\frac{di_{c3}}{dt} = -R_{PF}i_{c3} - d_{n3}v_{dc} - v_{CPF3} + v_{s3}$$
$$C_{dc}\frac{dv_{dc}}{dt} + \frac{v_{dc}}{R_{dc}} = d_{n1}i_{c1} + d_{n2}i_{c2} + d_{n3}i_{c3}. \quad (4)$$

The system of (4) is transformed into the synchronous orthogonal frame using the following general transformation matrix:

$$C_{dq}^{123} = \sqrt{\frac{2}{3}}\begin{bmatrix} \cos\theta & \cos(\theta - 2\pi/3) & \cos(\theta - 4\pi/3) \\ -\sin\theta & -\sin(\theta - 2\pi/3) & -\sin(\theta - 4\pi/3) \end{bmatrix} \quad (5)$$

where θ = ωt and the following equalities hold: Cdq123 =(C123dq)−1 = (C123dq)T .

Then, by applying dq transformation, the state space model of the system in the synchronous reference frame is given in the Appendix by (26).

This model is nonlinear because of the existence of multiplication terms between the state variables {id, iq, Vdc} and the switching state function {dnd, dnq}. However, the model is time invariant during a given switching state. Furthermore, the principle of operation of the SHPF requires that the three state variables have to be controlled independently. The interaction between the inner current loop and the outer dc bus voltage loop can be avoided by adequately separating their respective dynamics.

3.2 Harmonic Current Control

A fast inner current loop, and a slow outer dc voltage loop, is adopted. The first two equations in the model can be written as shown in the Appendix by (27). Note that the first and the

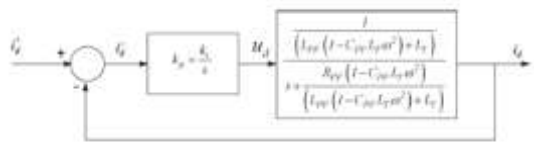

Fig. 2. Inner control loop of the current i_{sd}.

second time derivative TCR capacitor voltages have no significant negative impact on the performance of the proposed control technique because their coefficients are too low. Consequently, they can practically be ignored. Define the equivalent inputs by (28) as given in the Appendix. Thus, with this transformation, the decoupled dynamics of the current tracking is obtained. The currents id and iq can be controlled independently.

Furthermore, by using proportional integral compensation, a fast dynamic response and zero steady-state errors can be achieved. The expressions of the tracking controllers are

$$u_d = \left(L_{PF}(1 - C_{PF}L_T\omega^2) + L_T\right)\frac{di_d}{dt} + R_{PF}(1 - C_{PF}L_T\omega^2)i_d = k_p\tilde{i}_d + k_i\int \tilde{i}_d dt$$
$$u_q = \left(L_{PF}(1 - C_{PF}L_T\omega^2) + L_T\right)\frac{di_q}{dt} + R_{PF}(1 - C_{PF}L_T\omega^2)i_q = k_p\tilde{i}_q + k_i\int \tilde{i}_q dt \quad (6)$$

where ˜id = i∗ d− id and ˜iq = i∗ q− iq are current errors and i∗ d and i∗ q denote the reference signals of id and iq, respectively. The transfer function of the proportional–integral controllers is given as

$$G_{i1}(s) = \frac{U_d(s)}{\tilde{i}_d(s)} = k_{p1} + \frac{k_{i1}}{s}$$
$$G_{i2}(s) = \frac{U_q(s)}{\tilde{i}_q(s)} = k_{p2} + \frac{k_{i2}}{s}. \quad (7)$$

The inner control loop of the current id is shown in Fig. 2. The closed-loop transfer functions of the current loops are

$$\frac{I_d(s)}{I_d^*(s)} = \frac{k_{p1}}{A}\frac{\left(s + \frac{k_{i1}}{k_{p1}}\right)}{s^2 + \left(\frac{B + k_{p1}}{A}\right)s + k_{i1}}$$
$$\frac{I_q(s)}{I_q^*(s)} = \frac{k_{p2}}{A}\frac{\left(s + \frac{k_{i2}}{k_{p2}}\right)}{s^2 + \left(\frac{B + k_{p2}}{A}\right)s + k_{i2}} \quad (8)$$

where $A = L_{PF}(1 - C_{PF}L_T\omega^2) + L_T$ and $B = R_{PF}(1 - C_{PF}L_T\omega^2)$.

The closed-loop transfer functions of the current loops have the following form:

$$\frac{I_d(s)}{I_d^*(s)} = 2\zeta\omega_{ni}\frac{s + \frac{\omega_{ni}}{2\zeta}}{s^2 + 2\zeta\omega_{ni}s + \omega_{ni}^2} \quad (9)$$

where ωni is the outer loop natural angular frequency and ζ is the damping factor. For the optimal value of the damping factor

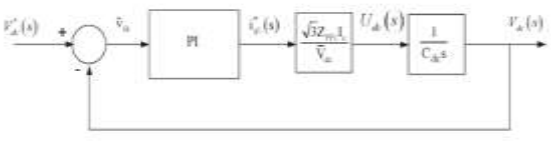

Fig. 3. Compensated voltage regulated model.

ζ =√2/2, the theoretical overshoot is 20.79%. The following design relations can be derived:

$$k_{p1} = k_{p2} = 2\zeta\omega_{ni}\left(L_{PF}(1 - C_{PF}L_T\omega^2) + L_T\right) - R_{PF}(1 - C_{PF}L_T\omega^2)$$
$$k_{i1} = k_{i2} = (L_{PF}(1 - C_{PF}L_T\omega^2) + L_T)\omega_{ni}^2.$$

The control law is given in the Appendix by (29) and (30). Note that the inputs qnd and qnq consist of a nonlinearity cancellation part and a linear decoupling compensation part.

3.3 DC Bus Voltage Regulation

In order to maintain the dc bus voltage level at a desired value, acting on iq can compensate the losses through the hybrid power filter components. The output of the controller is added to the q-component current reference iq as shown in Fig. 4. The
third equation in the model (6) is rewritten

$$C_{dc}\frac{dv_{dc}}{dt} + \frac{v_{dc}}{R_{dc}} = d_{nq}i_q. \quad (10)$$

The three-phase filter currents are given by

$$\begin{bmatrix} i_{c1} \\ i_{c2} \\ i_{c3} \end{bmatrix} = \sqrt{\frac{2}{3}}i_q \begin{bmatrix} -\sin\theta \\ -\sin\left(\theta - \frac{2\pi}{3}\right) \\ -\sin\left(\theta - \frac{2\pi}{3}\right) \end{bmatrix}. \quad (11)$$

The fundamental filter rms current I_c is

$$I_c = \frac{i_q}{\sqrt{3}}. \quad (12)$$

The q-axis active filter voltage v_{Mq} is expressed as

$$v_{Mq} = q_{nq}v_{dc} = -Z_{PF1}i_{q1}^* \quad (13)$$

where Z_{PF1} is the impedance of the passive filter at 60 Hz and i_{q1}^* is a dc component.

An equivalent input u_{dc} is defined as

$$u_{dc} = q_{nq}i_q. \quad (14)$$

The control effort of the dc voltage loop is deduced

$$i_{q1}^* = \frac{v_{dc}}{-Z_{PF1}i_q}u_{dc}. \quad (15)$$

The dc component will force the SHPF-TCR compensator to generate or to draw a current at the fundamental frequency.

To regulate the dc voltage v_{dc}, the error $\tilde{v}_{dc} = v_{dc}^* - v_{dc}$ is passed through a PI-type controller given by

$$u_{dc} = k_1\tilde{v}_{dc} + k_2\int \tilde{v}_{dc}\,dt. \quad (16)$$

Fig. 3 illustrates the outer control loop of the dc bus voltage.

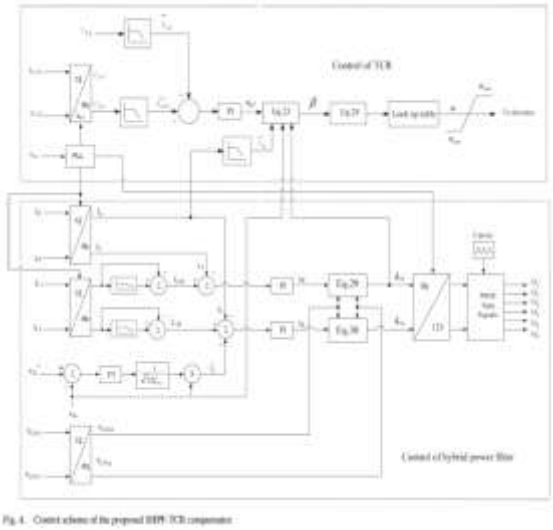

The response of the dc bus voltage loop is a second-order transfer function and has the following form:

$$\frac{V_{dc}(s)}{V_{dc}^*(s)} = 2\zeta\omega_{nv}\frac{s + \frac{\omega_{nv}}{2\zeta}}{s^2 + 2\zeta\omega_{nv}s + \omega_{nv}^2}. \quad (17)$$

The closed-loop transfer function of dc bus voltage regulation is given as follows:

$$\frac{V_{dc}(s)}{V_{dc}^*(s)} = \frac{\frac{\sqrt{3}Z_{PF1}k_pI_c}{V_{dc}C_{dc}}s + \frac{\sqrt{3}Z_{PF1}k_iI_c}{V_{dc}C_{dc}}}{s^2 + \frac{\sqrt{3}Z_{PF1}k_pI_c}{V_{dc}C_{dc}}s + \frac{\sqrt{3}Z_{PF1}k_iI_c}{V_{dc}C_{dc}}} \quad (18)$$

where V dc is the average value of the dc voltage which is equal to 50 V. The proportional k1 and integral k2 gains are then obtained as follows: k1 2ζωnv(V dcCdc/√3ZPF1Ic), and k2 =ω2nv(V dcCdc/√3ZPF1Ic). By designing the dc bus voltage
loop much slower than the current one, there would not be any interaction between the two loops. The proposed nonlinear controller of the proposed SHPFTCR compensator is shown in Fig. 4.

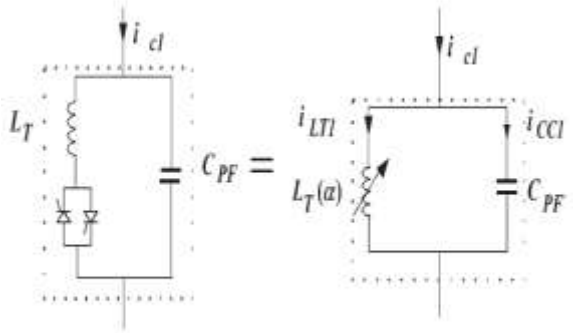

Fig. 5. TCR equivalent circuit.

3.4 MODELING OF TCR

Fig. 5 shows the TCR equivalent circuit. Using Kirchhoff's voltage law, the following equations in 123 reference frame are obtained:

$$v_{s1} = L_T \frac{di_{LT1}}{dt} + L_{PF} \frac{di_{c1}}{dt} + R_{PF} i_{c1} + d_{n1} v_{dc}$$

$$v_{s2} = L_T \frac{di_{LPF2}}{dt} + L_{PF} \frac{di_{c2}}{dt} + R_{PF} i_{c2} + d_{n2} v_{dc}$$

$$v_{s3} = L_T \frac{di_{LPF3}}{dt} + L_{PF} \frac{di_{c3}}{dt} + R_{PF} i_{c3} + d_{n3} v_{dc}. \quad (19)$$

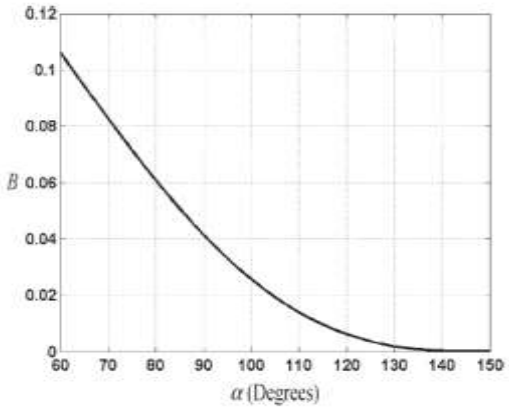

Fig. 6. Susceptance versus firing angle.

Applying Park's transformation, one obtains

$$L_T(\alpha) \frac{di_{LTd}}{dt} = L_T(\alpha) \omega i_{LTq} + L_{PF} \omega i_q - L_{PF} \frac{di_d}{dt} - R_{PF} i_d - d_{nd} v_{dc} + v_d$$

$$L_T(\alpha) \frac{di_{LTq}}{dt} = -L_T(\alpha) \omega i_{LTd} - L_{PF} \omega i_d - L_{PF} \frac{di_q}{dt} - R_{PF} i_q - d_{nq} v_{dc} + v_q. \quad (20)$$

The reactive part is chosen to control the reactive current so that $v_q = 0$ and $L_f(\alpha) \omega i_{LTd} = 0$

$$\frac{di_{LTq}}{dt} = B(\alpha) \omega \left[-L_{PF} \omega i_d - L_{PF} \frac{di_q}{dt} - R_{PF} i_q - d_{nq} v_{dc} \right] \quad (21)$$

where $B(\alpha) = 1/L_F(\alpha)\omega$ is the susceptance.

An equivalent input u_{qT} is defined as

$$u_{qT} = \frac{di_{LTq}}{dt}. \quad (22)$$

According to this expression, one deduces

$$B(\alpha) = \frac{u_{qT}}{\omega \left[-L_{PF} \omega i_d - L_{PF} \frac{di_q}{dt} - R_{PF} i_q - d_{nq} v_{dc} \right]}. \quad (23)$$

On the other hand, the equivalent inductance is given by

$$L_{PF}(\alpha) = L_{PF} \frac{\pi}{2\pi - 2\alpha + \sin(2\alpha)}. \quad (24)$$

The susceptance is given by

$$B(\alpha) = B \frac{2\pi - 2\alpha + \sin(2\alpha)}{\pi} \quad (25)$$

where $B = 1/L_{PF}\omega_0$.

Fig. 6 illustrates the susceptance versus firing angle.

4. SIMULATION RESULTS

4.1 Simulation Dia. of SHPF-TCR

Below Fig shows the Simulation Dia. of SHPF-TCR.

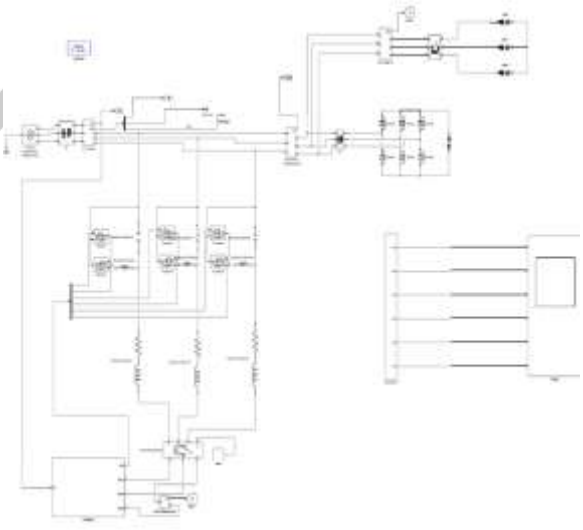

The system parameters are given in Table II. Simulations were performed numerically using the "Power System Blockset" simulator operating under Matlab/Simulink environment, in order to verify the operation of the proposed SHPF-TCR compensator using the nonlinear control scheme shown in Figs. 1 and 5.

Table II	
Specification Parameters	
Line to Line source voltage and frequency	line to line Voltage=230, Fs=50 Hz
Line Impedance	Ls=0.5mH,Rs=0.1 ohm
Non Linear load	LL1=10 mH,RL1=27 ohm
Linear load	LL1=20 mH,RL1=27 ohm
Passive Filter parameters	Lpf= 1.2mH, Cpf=240μF
Active filter parameters	Cdc=3000μF, Rdc=1K ohm
DC bus voltage of APF of SHAF	Vdc=50 V
Switching Frequency	1920 Hz
Inner Controller parameters	Kp1=Kp2=43.38 Ki1=Ki2=37408
Outer controller parameters	K1=0.26 K2=42
Cut off frequency of the low pass filters	Fc=70Hz
TCR inductance	LT=25mH

We have observed the waveforms for both the Nonlinear load and Reactive load with and without compensation where, Vs1=Supply Voltage, Is1= Supply current,IL1= Load current of Non linear load, IL2= Load current of reactive load, Ic1= Injected current for compensation, Vdc=Injected voltage for compensation

Waveforms observed for Tome Period 0 to 1 Sec, Non linear Operational time 0 to 1 sec, reactive load operational time 0.5 to sec, SHPF-TCR operational time 0.7 to 1 sec.

It is observed that the supply current before compensation was quite distorted and has a THD of 25.31%; however, its THD is reduced to 0.84% after compensation. The compensated source current shown in this figure suggests that the proposed SHPF-TCR compensator can effectively compensate the load-generated harmonics and reactive power exchanged by both loads.

4.2 Waveforms of Non Linear Load without compensation

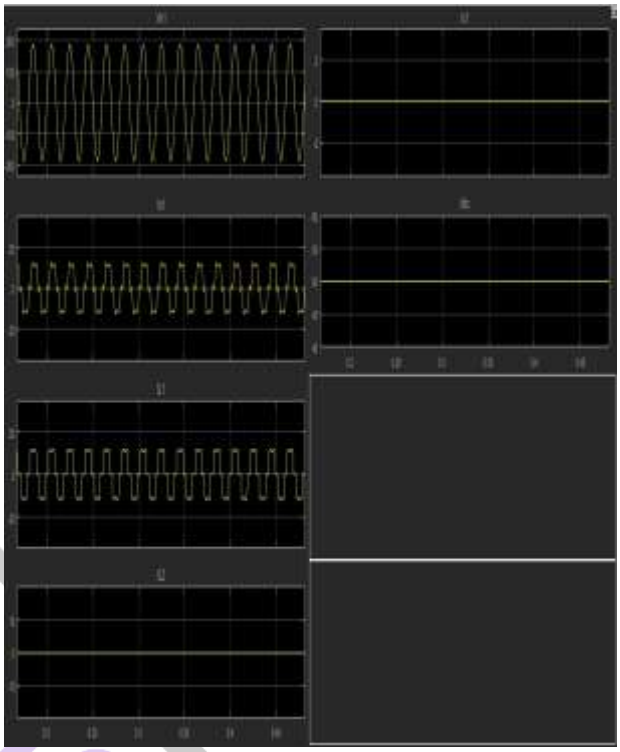

4.3 Waveforms of Non Linear Load+ Reactive Load without compensation

4.4 Waveforms of Non Linear Load+ Reactive Load with compensation

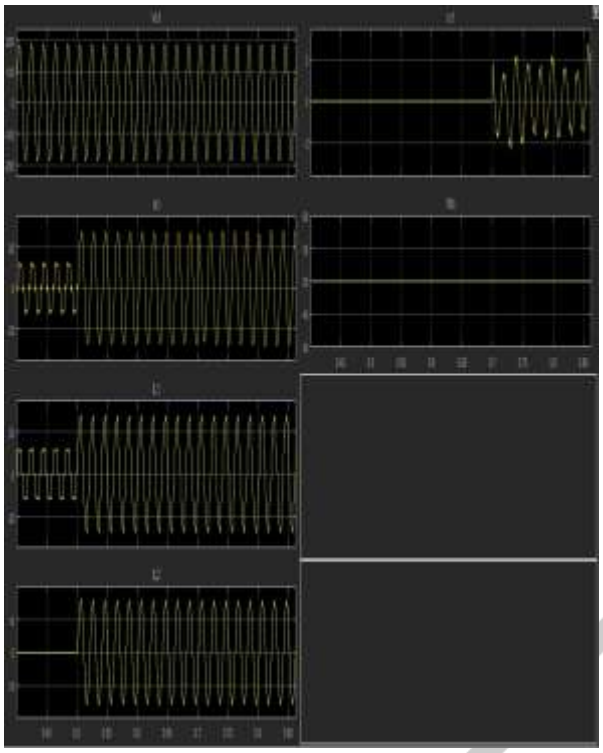

4.5 THD of Non Linear Load without compensation

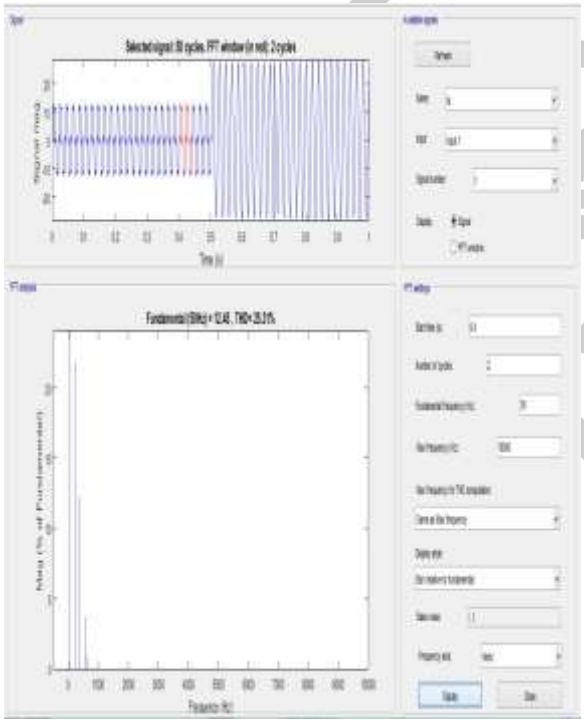

4.6 THD of Non Linear Load + Reactive Load with compensation

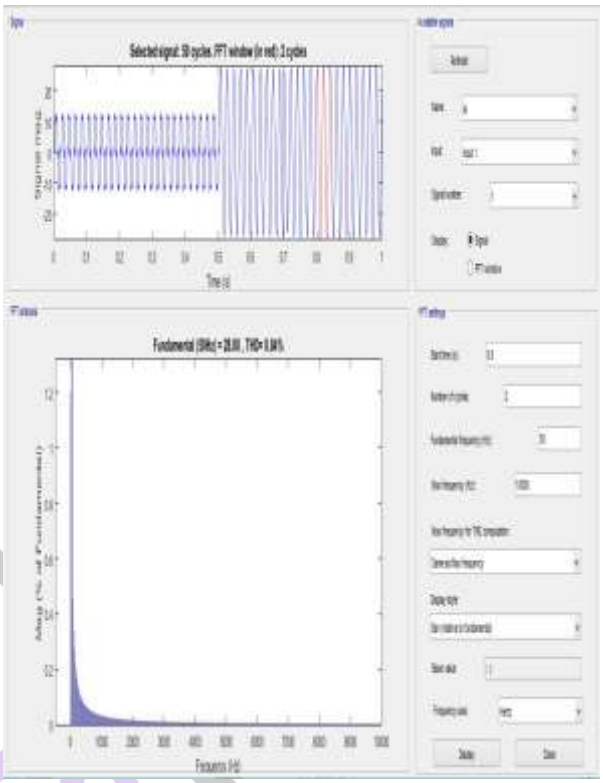

5. EXPERIMENTAL RESULTS

The following tests are performed on a 3.5-kVA laboratory prototype of the SHPF-TCR compensator used to compensate harmonics and reactive power of loads. The nonlinear control system was implemented on a dSPACE DS 1104 controller board, supported by a Matlab/Simulink Real-Time Workshop environment. The component values given in Table I were used for both simulation and experimentation. The set of loads consists of a diode rectifier and a star-connected combination resistive and inductive loads. The experimental setup used to test the dynamic performance of the SHPF-TCR compensator has the following combined harmonic and reactive power type of loads.

1) A three-phase diode rectifier followed by inductor LL1 =10 mH in series with a resistor RL1 = 40Ωis used as the harmonic-produced load.

2) A three-phase star-connected resistive inductive load with inductor LL2 = 20 mH and resistor RL2 = 27 Ω is used to cause current to lag voltage and to make up a mixed load together with the three-phase harmonic generated load.

To verify the proposed nonlinear control algorithm performance, four different operating conditions are considered: 1) steady-state performance of the SHPF-TCR compensator with a harmonic-produced load; 2) dynamic performance of the SHPF-TCR compensator with harmonic-generated load;
3) steady-state performance of the SHPF-TCR compensator with the harmonic and reactive power type of loads; and 4) dynamic performance of the system with the harmonic and reactive power type of loads.

5.1 Steady-State Response of System with Harmonic-Generated Load

Fig. 12 shows the steady-state experimental results of the proposed SHPF-TCR compensator for harmonic compensation

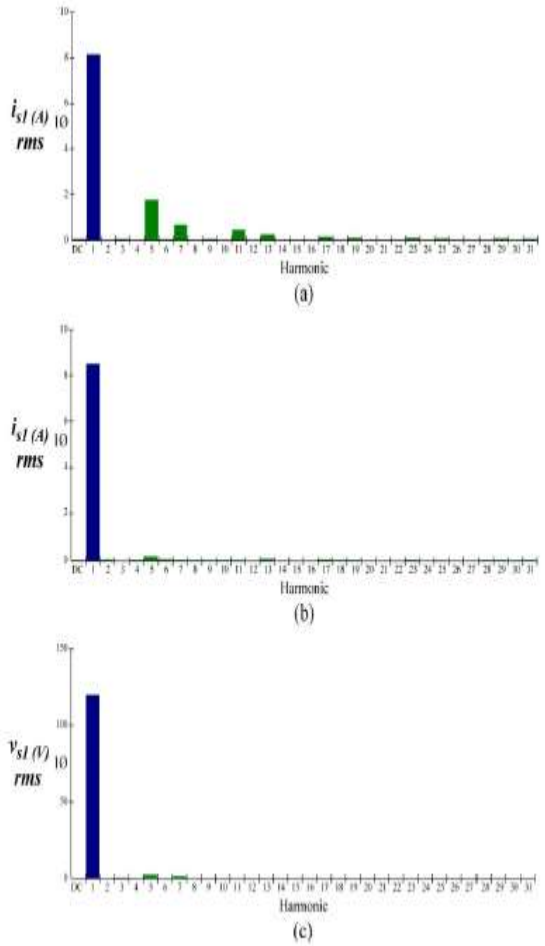

Fig. 13. Harmonic spectrums of the source current and voltage in phase 1. (a) Source current before compensation. (b) Source current after compensation. (c) Source voltage.

with a load for phase 1. In this figure, the supply voltage (vs1), supply current (is1), load current (iL1), and SHPF-TCR current (ic1) are depicted. It can be seen that the source current has become sinusoidal and in phase with the source voltage. The harmonic spectrum of the supply current before and after compensation and the supply voltage after compensation for phase 1 have been given in Figs. 13(a), (b), and 14(c), respectively. The THD of the supply current is brought dow from 26% before compensation to 3% after compensation. The THD of the supply voltage after compensation is 2.5%. The harmonic spectrums are recorded on a FLUKE 43B power quality analyzer.

5.2 Transient Response of SHPF-TCR Compensator to Harmonic-Produced Load Variation

To test the dynamic performance of the proposed nonlinear control, a step increase of 100% and a decrease of 100% in the harmonic-produced load were made. Fig. 14(a) and (b) shows the transient responses of the SHPF-TCR compensator adopting the nonlinear control. At the transition period, the dc bus voltage falls or rises below its steady-state value when the SHPF-TCR compensator supplies or absorbs extra active power or from the load, respectively. The SHPF-TCR compensator maintains compensation during the transient instants. Thus, the harmonic components of the load current are fully compensated by the system so that the line current is almost a sinusoidal waveform with unity PF.

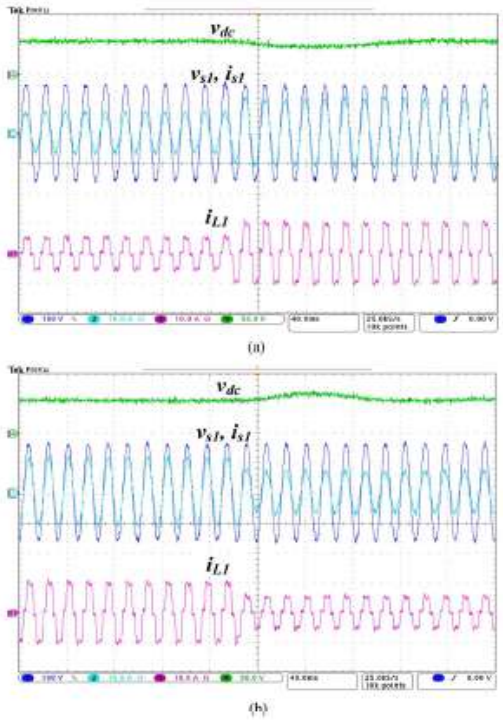

Fig. 14. Dynamic response of the proposed SHPF-TCR compensator under varying harmonic-produced load conditions. (a) Step increase of the load current. (b) Step decrease of the load current.

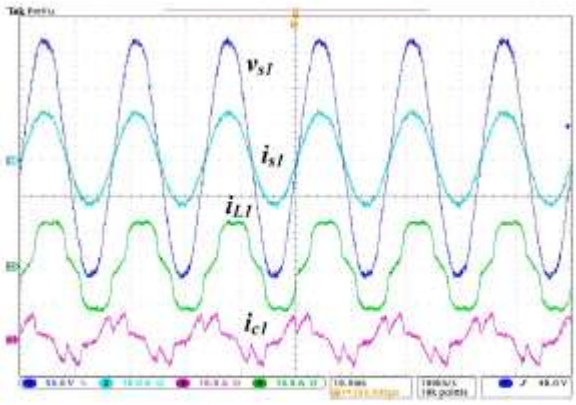

Fig. 15. Steady-state response of the proposed SHPF-TCR compensator with harmonic and reactive power type of loads.

5.3 Steady-State Harmonic and Reactive Power Compensation

A combination of a three-phase diode-bridge ac–dc converter with an R−L load connected at the dc side and a three-phase

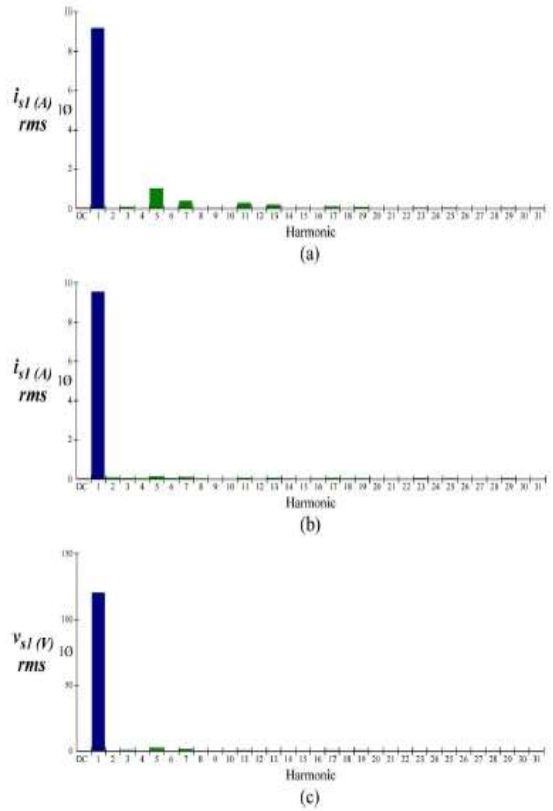

Fig. 16. Harmonic spectrums of the source current and voltage in phase 1. (a) Source current before compensation. (b) Source current after compensation. (c) Source voltage.

star-connected resistive–inductive load is chosen to study the transient operation of the SHPF-TCR system for harmonic and reactive power compensation. The PF of the reactive load is 0.96. Fig. 15 shows the steady-state performance of the proposed SHPF-TCR compensator employing the proposed nonlinear control method for the simultaneous compensation of harmonics and reactive power for phase 1. The supply voltage (vs1), the supply current (is1), the load current (iL1) and the SHPF-TCR compensator current (ic1) are shown in this figure. The frequency analyses of supply voltage and supply current before and after compensation are shown in Fig. 16(a)–(c). The THD of the supply current is brought down from 15% before compensation to 2.6% after compensation. The THD of the supply voltage after compensation is 2.5%.

The steady-state performance of the TCR providing reactive power compensation is shown in Fig. 17. The waveforms shown in this figure are the phase-1 source current (is1), load current (iL1), hybrid filter current (ic1), and TCR current (iLt1). From the experimental results, one can observe that the harmonic currents and reactive power could be effectively compensated with the SHPF-TCR compensator. The source current is close to sinusoidal and kept in phase with the source voltage. Moreover, harmonics generated naturally by the TCR have two possible paths, the parallel capacitor connected with the TCR or the active filter. Since the active filter controller is set to compensate only load harmonics, the latter act as high impedance to TCR
current harmonics, obliging these harmonics to flow through the capacitor. Therefore, one cannot see these harmonics flowing through the source or the load.

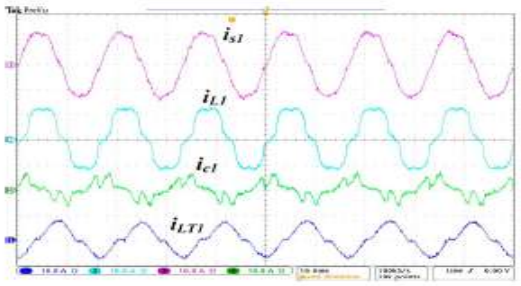

Fig. 17. TCR providing reactive power compensation in steady-state mode.

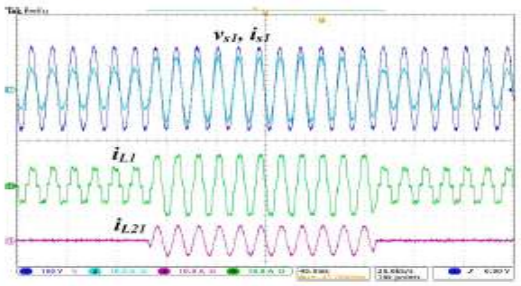

Fig. 18. Dynamic response of the proposed SHPF-TCR compensator under varying reactive power type of load conditions.

5.4 Reactive Power and Harmonic Type of Load Perturbation Response of SHPF-TCR Compensator

Fig. 18 shows the transient waveforms of the SHPF-TCR compensator during the sudden variation of the reactive power and harmonic type of loads. It is found that, for a change of load current, the supply current always maintains its sinusoidal shape while being in phase with the supply voltage. These results confirm the fast dynamic performance and the ability of the proposed configuration adopting the nonlinear control strategy to compensate suitably the harmonics and reactive power for a rapid change in the load current. The THDs of the load current before and after the transient %, respectively. The PF of the reactive load is 0.96. The TCR is used to realize variable inductance for compensating the reactive power.

This latter suffers from resonance which possibly occurs between its inductance, source/load impedance, and PF correction capacitors used in industrial applications. Passive filters suffer from resonance problems and tuning problems due to component tolerances. The problem with the active filters arises, particularly in high-power loads, when the current needed and voltage rating of the active filters are high. Combining the advantages of the passive filter and active filter, hybrid active filter topologies can reduce the voltampere rating of the APF.

$$\frac{di_d}{dt} = \frac{1}{(L_{TF}(1-C_{TF}L_{TF}\omega^2)+L_T)}\Big[-R_{TF}(1-C_{TF}L_{TF}\omega^2)i_d+\omega(L_{TF}(1-C_{TF}L_{TF}\omega^2)+L_T)i_q-2\omega C_{TF}L_T\frac{dv_{CTFd}}{dt}$$
$$+C_{TF}L_T\frac{d^2v_{CTFd}}{dt^2}-(1-C_{TF}L_T\omega^2)d_{sd}v_{dc}+(1-C_{TF}L_T\omega^2)v_d\Big]$$

$$\frac{di_q}{dt} = \frac{1}{(L_{TF}(1-C_{TF}L_{TF}\omega^2)+L_T)}\Big[-R_{TF}(1-C_{TF}L_{TF}\omega^2)i_q-\omega(L_{TF}(1-C_{TF}L_{TF}\omega^2)+L_T)i_d+2\omega C_{TF}L_T\frac{dv_{CTFd}}{dt}$$
$$+C_{TF}L_T\frac{d^2v_{CTFq}}{dt^2}-(1-C_{TF}L_T\omega^2)d_{sq}v_{dc}+(1-C_{TF}L_T\omega^2)v_q\Big]$$

$$\frac{dv_{dc}}{dt} = \frac{d_{sd}}{C_{dc}}i_d+\frac{d_{sq}}{C_{dc}}i_q-\frac{v_{dc}}{R_{dc}C_{dc}} \quad (26)$$

$$\frac{di_d}{dt} + \frac{R_{TF}(1-C_{TF}L_T\omega^2)}{(L_{TF}(1-C_{TF}L_{TF}\omega^2)+L_T)}i_d$$
$$= \frac{1}{(L_{TF}(1-C_{TF}L_{TF}\omega^2)+L_T)}\Big[\omega(L_{TF}(1-C_{TF}L_{TF}\omega^2)+L_T)i_q-2\omega C_{TF}L_T\frac{dv_{CTFd}}{dt}+C_{TF}L_T\frac{d^2v_{CTFd}}{dt^2}$$
$$-(1-C_{TF}L_T\omega^2)d_{sd}v_{dc}+(1-C_{TF}L_T\omega^2)v_d\Big]$$

$$\frac{di_q}{dt} + \frac{R_{TF}(1-C_{TF}L_T\omega^2)}{(L_{TF}(1-C_{TF}L_{TF}\omega^2)+L_T)}i_q$$
$$= \frac{1}{(L_{TF}(1-C_{TF}L_{TF}\omega^2)+L_T)}\Big[-\omega(L_{TF}(1-C_{TF}L_{TF}\omega^2)+L_T)i_d+2\omega C_{TF}L_T\frac{dv_{CTFq}}{dt}+C_{TF}L_T\frac{d^2v_{CTFq}}{dt^2}$$
$$-(1-C_{TF}L_T\omega^2)d_{sq}v_{dc}+(1-C_{TF}L_T\omega^2)v_q\Big] \quad (27)$$

$$v_d = \frac{1}{(L_{TF}(1-C_{TF}L_{TF}\omega^2)+L_T)}\left[\omega(L_{TF}(1-C_{TF}L_{TF}\omega^2)+L_T)i_q-(1-C_{TF}L_T\omega^2)d_{sd}v_{dc}+(1-C_{TF}L_T\omega^2)v_d\right]$$

$$v_q = \frac{1}{(L_{TF}(1-C_{TF}L_{TF}\omega^2)+L_T)}\left[-\omega(L_{TF}(1-C_{TF}L_{TF}\omega^2)+L_T)i_d-(1-C_{TF}L_T\omega^2)d_{sq}v_{dc}+(1-C_{TF}L_T\omega^2)v_q\right] \quad (28)$$

$$d_{sd} = \frac{1}{(1-C_{TF}L_T\omega^2)v_{dc}}\left[\omega(L_{TF}(1-C_{TF}L_{TF}\omega^2)+L_T)i_q+(1-C_{TF}L_T\omega^2)v_d-(L_{TF}(1-C_{TF}L_T\omega^2)+L_T)i_d\right] \quad (29)$$

$$d_{sq} = \frac{1}{(1-C_{TF}L_T\omega^2)v_{dc}}\left[-\omega(L_{TF}(1-C_{TF}L_{TF}\omega^2)+L_T)i_d+(1-C_{TF}L_T\omega^2)v_q-(L_{TF}(1-C_{TF}L_T\omega^2)+L_T)i_q\right] \quad (30)$$

In the proposed SHPF-TCR combination, the major part of the compensation is supported by the passive filter while the APF improves the filtering characteristics and damps the resonance. Indeed, the combined system can greatly reduce problems of using only TCR or shunt active filters and is suitable for harmonic and reactive power compensation for large voltampere-rated loads in power systems because the required voltampere rating of the APF used in the hybrid power filter is considerably smaller than a conventional shunt APF. Also, the obtained results illustrate how the compensation characteristics of the TCR used to compensate reactive power in a large industrial power distribution system can be improved by connecting a hybrid power filter, which eliminates current harmonics. In addition, the proposed topology lends itself to retrofit applications with the existing TCR and passive filter.

6. CONCLUSION

A advanced control logic based HAPF controller has been designed for stabilization of power systems. The control has been tested on several load conditions with transient/ dynamic/steady state conditions. In this paper, a SHPF-TCR compensator of a TCR and a SHPF has been proposed to achieve harmonic elimination and reactive power compensation. A proposed nonlinear control scheme of a SHPF-TCR compensator has been established, simulated, and implemented by using the digital real time controller board of dSPACE. The shunt active filter and SPF have a complementary function to improve the performance of filtering and to reduce the power rating requirement of an active filter. It has been found that the SHPF-TCR compensator can effectively eliminate current harmonic and reactive power compensation during steady and transient operating conditions for a variety of loads. It has been shown that the system has a fast dynamic response, has good performance in both steady-state and transient operations, and is able to reduce the THD of supply currents well below the limit of 5% of the IEEE-519 standard.

REFERENCES

[1] A. Hamadi, S. Rahmani, and K. Al-Haddad, "A hybrid passive filter configuration for VAR control and harmonic compensation," IEEE Trans. Ind. Electron., vol. 57, no. 7, pp. 2419–2434, Jul. 2010.

[2] P. Flores, J. Dixon, M. Ortuzar, R. Carmi, P. Barriuso, and L. Moran, "Static Var compensator and active power filter with power injection capability, using 27-level inverters and photovoltaic cells," IEEE Trans. Ind. Electron., vol. 56, no. 1, pp. 130–138, Jan. 2009.

[3] H. Hu, W. Shi, Y. Lu, and Y. Xing, "Design considerations for DSPcontrolled 400 Hz shunt active power filter in an aircraft power system," IEEE Trans. Ind. Electron., vol. 59, no. 9, pp. 3624–3634, Sep. 2012.

[4] X. Du, L. Zhou, H. Lu, and H.-M. Tai, "DC link active power filter for three-phase diode rectifier," IEEE Trans. Ind. Electron., vol. 59, no. 3, pp. 1430–1442, Mar. 2012.

[5] M. Angulo, D. A. Ruiz-Caballero, J. Lago, M. L. Heldwein, and S. A. Mussa, "Active power filter control strategy with implicit closedloop current control and resonant controller," IEEE Trans. Ind. Electron., vol. 60, no. 7, pp. 2721–2730, Jul. 2013.

[6] X. Wang, F. Zhuo, J. Li, L. Wang, and S. Ni, "Modeling and control of dual-stage high-power multifunctional PV system in d-q-0 coordinate," IEEE Trans. Ind. Electron., vol. 60, no. 4, pp. 1556–1570, Apr. 2013.

[7] J. A. Munoz, J. R. Espinoza, C. R. Baier, L. A. Moran, E. E. Espinosa, P. E. Melin, and D. G. Sbarbaro, "Design of a discrete-time linear control
strategy for a multicell UPQC," IEEE Trans. Ind. Electron., vol. 59, no. 10, pp. 3797–3807, Oct. 2012.

[8] L. Junyi, P. Zanchetta, M. Degano, and E. Lavopa, "Control design and implementation for high performance shunt active filters in aircraft power grids," IEEE Trans. Ind. Electron., vol. 59, no. 9, pp. 3604–3613, Sep. 2012.

[9] Y. Tang, P. C. Loh, P. Wang, F. H. Choo, F. Gao, and F. Blaabjerg, "Generalized design of high performance shunt active power filter withn output LCL filter," IEEE Trans. Ind. Electron., vol. 59, no. 3, pp. 1443– 1452, Mar. 2012.

[10] Z. Chen, Y. Luo, and M. Chen, "Control and performance of a cascaded shunt active power filter for aircraft electric power system," IEEE Trans. Ind. Electron., vol. 59, no. 9, pp. 3614–3623, Sep. 2012.

[11] S. Rahmani, A. Hamadi, K. Al-Haddad, and A. I. Alolah, "A DSP-based implementation of an instantaneous current control for a three-phase shunt hybrid power filter," J. Math. Comput. Simul.—Model. Simul. Elect. Mach., Convert. Syst., vol. 91, pp. 229–248, May 2013.

[12] C. S. Lam, W. H. Choi, M. C. Wong, and Y. D. Han, "Adaptive dc-link voltage-controlled hybrid active power filters for reactive power compensation," IEEE Trans. Power Electron., vol. 27, no. 4, pp. 1758–1772, Apr. 2012.

[13] A. Hamadi, S. Rahmani, and K. Al-Haddad, "Digital control of hybrid power filter adopting nonlinear control approach," IEEE Trans. Ind. Informat., to be published.

[14] A. Bhattacharya, C. Chakraborty, and S. Bhattacharya, "Parallel connected shunt hybrid active power filters operating at different switching
frequencies for improved performance," IEEE Trans. Ind. Electron., vol. 59, no. 11, pp. 4007–4019, Nov. 2012.

[15] S. Rahmani, A. Hamadi, N.Mendalek, and K. Al-Haddad, "A new control
technique for three-phase shunt hybrid power filter," IEEE Trans. Ind.